

# Efficient Camera Exposure Control for Visual Odometry via Deep Reinforcement Learning

Shuyang Zhang<sup>1</sup>, Jinhao He<sup>2</sup>, Yilong Zhu<sup>1</sup>, Jin Wu<sup>1</sup> and Jie Yuan<sup>1</sup>

**Abstract**—The stability of visual odometry (VO) systems is undermined by degraded image quality, especially in environments with significant illumination changes. This study employs a deep reinforcement learning (DRL) framework to train agents for exposure control, aiming to enhance imaging performance in challenging conditions. A lightweight image simulator is developed to facilitate the training process, enabling the diversification of image exposure and sequence trajectory. This setup enables completely offline training, eliminating the need for direct interaction with camera hardware and the real environments. Different levels of reward functions are crafted to enhance the VO systems, equipping the DRL agents with varying intelligence. Extensive experiments have shown that our exposure control agents achieve superior efficiency—with an average inference duration of 1.58 ms per frame on a CPU—and respond more quickly than traditional feedback control schemes. By choosing an appropriate reward function, agents acquire an intelligent understanding of motion trends and anticipate future illumination changes. This predictive capability allows VO systems to deliver more stable and precise odometry results. The codes and datasets are available at [https://github.com/ShuyangUni/drl\\_exposure\\_ctrl](https://github.com/ShuyangUni/drl_exposure_ctrl).

## I. INTRODUCTION

Effective camera exposure control is crucial for dynamic robotics applications like visual odometry (VO), characterized by complex lighting. Inadequate exposure control may fail to promptly adjust to the rapid changes in lighting or field of view, resulting in protracted periods of over-saturation (under-exposure or over-exposure) and consequent loss of critical information, which poses safety risks to the robots.

Current camera exposure control methods for VO tasks are principally categorized into gradient-based and function-fitting approaches. Gradient-based methods employ a differentiable image metric to guide exposure optimization and use a feedback control mechanism to iteratively refine exposure settings, ensuring stability and cost-effectiveness. However, these methods are limited to the requirement of differentiable metrics and typically require multiple frames to achieve optimal exposure due to the inherent lag of the feedback control system. In contrast, function-fitting methods establish a relationship between the image metric and exposure, typically offering a one-shot solution that responds instantly and can accommodate any metric design, albeit at the cost of significant computational resources.

<sup>1</sup>S. Zhang, Y. Zhu, J. Wu and J. Yuan are with the Department of Electronic and Computer Engineering, the Hong Kong University of Science and Technology, Clear Water Bay, Kowloon, Hong Kong SAR, China. (email: szhangcy@connect.ust.hk)

<sup>2</sup>J. He is with the Thrust of Robotics and Autonomous Systems, the Hong Kong University of Science and Technology (GZ), Guangzhou, China.

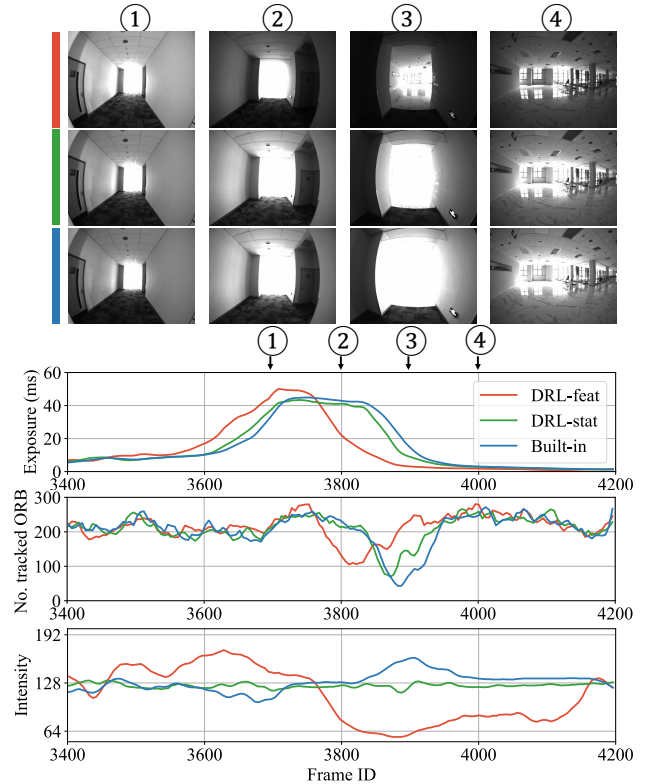


Fig. 1. An illustration of drastic illumination change in our *Corridor* sequence. Our DRL-based method with feature-level rewards (**DRL-feat**) exhibits a high-level comprehension of lighting and motion, surpassing the traditional method (**Built-in**) and DRL method with image statistic-level rewards (**DRL-stat**). The agent **DRL-feat** predicts the impending over-exposure event and preemptively reduces the exposure. While this adjustment temporarily decreases the number of tracked feature points, it effectively prevents a more severe failure in subsequent frames.

Existing exposure control methods often struggle under challenging conditions. Transitions through environments with drastically differing illumination, such as tunnels [1], can destabilize the frontend of VO systems: Gradient-based methods produce over-saturated images due to delays in parameter updates due to their feedback mechanisms. Function-fitting methods, despite their rapid response, result in significant disparities between adjacent frames. Both methods may ultimately lead to the failure of interframe tracking. Developing a robust camera exposure control method that can intelligently manage such extreme conditions will markedly improve the performance of VO systems.

In this study, we leverage a deep reinforcement learning (DRL) framework to enhance the system’s intelligence and robustness in extreme lighting conditions. DRL inte-

grates high-level information directly into its reward design and efficient real-time control outputs. As a data-driven approach, DRL assimilates specific task and scenario requirements from data, enabling intelligent and adaptive responses. Several existing methods [1], [2] have pursued similar avenues. However, these methods necessitate online interactions during the training phase, relying on specially designed devices to interact with real-world environments, which introduces challenges in implementation and sample efficiency—a common limitation in DRL applications. The contributions of our work include:

- A DRL-based camera exposure control solution. The exposure control challenge is divided into two subtasks, enabling completely offline DRL operations without the necessity for online interactions.
- An lightweight image simulator based on imaging principles, significantly enhances the data efficiency and simplifies the complexity of DRL training.
- A study on reward function design with various levels of information. The trained agents are equipped with different intelligence, enabling them to deliver exceptional performance in challenging scenarios.
- Sufficient experimental evaluation, which demonstrates that our exposure control method improves the performance of VO tasks, and achieves faster response speed and reduced time consumption.

## II. RELATED WORK

### A. Optimization-based Exposure Control

Traditional exposure control methods are commonly conceptualized as optimization problems, addressed through either *gradient-based* or *function-fitting* techniques.

Gradient-based methods [3], [4], [5] compute the gradient of the image metric relative to exposure to determine the direction for parameter updates. These methods employ iterative optimization to refine exposure settings progressively. Shim *et al.* [3] applied  $\gamma$ -correction to simulate exposure variations, assessing image gradient magnitudes. The target exposure is relatedly determined by the gamma value derived by a fifth-order polynomial. Zhang *et al.* [4] enhanced Shim’s metric and rigorously validated their derivatives. Han *et al.* [5] combined gradient-based iterative search with image simulations, integrating optical flow to evaluate camera self-motion, thus enabling adjustments to gain and exposure time to mitigate motion blur. These methods typically exhibit *reactive* behavior, adjusting only in response to changes in scene conditions, which can lead to over-saturation in dynamically lit environments.

Function-fitting methods [6], [7] utilize synthetic imaging techniques to generate images at varied exposure levels, targeting global optimality directly. Kim *et al.* [6] developed a mixed image quality metric and produced synthetic images from a fixed exposure seed image, with Bayesian optimization to simultaneously refine exposure time and gain settings. Zhang *et al.* [7] integrated image bracketing patterns with synthetic techniques to periodically survey a high dynamic

range (HDR) spectrum of the scene, thereby improving the capture of scene irradiance. Function-fitting approaches provide rapid responses, potentially offering optimal settings from a single image capture; however, they require significant computational resources due to the exhaustive global optimization process.

### B. Reinforcement Learning-based Exposure Control

Recent advancements in deep reinforcement learning has markedly broadened their applications in real-world robotic tasks, including locomotion control [8], [9], perception [10], [11], and decision making [12], [13].

Existing DRL-based exposure control methods [1], [2] suffer the **online** training scheme, which is inefficient and in the risk of non-convergence. Tomasi *et al.* [1] utilized a deep convolutional neural network (CNN) to dynamically adjust camera gain and exposure time settings. Faced with the challenge of directly labeling optimal exposure parameters, they devised a self-supervised labeling technique using dual cameras and a specialized capture pattern. However, their approach of online data collection combined with offline agent training presents complexities and inefficiencies in implementation. Additionally, the infrequent policy updates within their system may hinder the generalization capabilities of the agent. Lee *et al.* [2] proposed a device-specific method to facilitate online training. They vectorized input images to eliminate CNN modules, thereby reducing model complexity. They introduced a progressive lighting curriculum that incrementally exposed the agent to increasingly complex training scenarios, which streamlined the training process. Their lightweight agent exhibited improved performance across various visual tasks. Nonetheless, the dependence on a specialized stable device limits their method’s generalizability and fails to address camera motion. Moreover, their approach to image vectorization sacrifices essential high-level visual information, such as feature detection and tracking.

In this study, we develop a DRL-based camera exposure control method specifically designed for VO systems. Our approach utilizes cameras equipped with a Sequencer mode, a bracketing imaging pattern that captures images at varying exposures, a feature prevalent in advanced machine vision cameras such as the FLIR Blackfly S<sup>1</sup> and Basler ACE<sup>2</sup>. We leverage this bracketing pattern alongside image synthesis techniques to construct an environment simulator for training exposure control agents. By introducing an intermediary exposure parameter, we dissect the exposure control problem into a cascading dual-module pipeline. The first module determines the optimal exposure, facilitating entirely **offline** training via our simulator. The second module implements a rule-based strategy to allocate the optimal exposure to exposure time and gain, interfacing directly with camera hardware. The environment simulator enhances the reward function by integrating multiple information tiers, thereby enabling agents to exhibit varied levels of intelligence within the VO systems.

<sup>1</sup><https://www.flir.com/products/blackfly-s-usb3/>

<sup>2</sup><https://www.baslerweb.com/en/cameras/ace/>

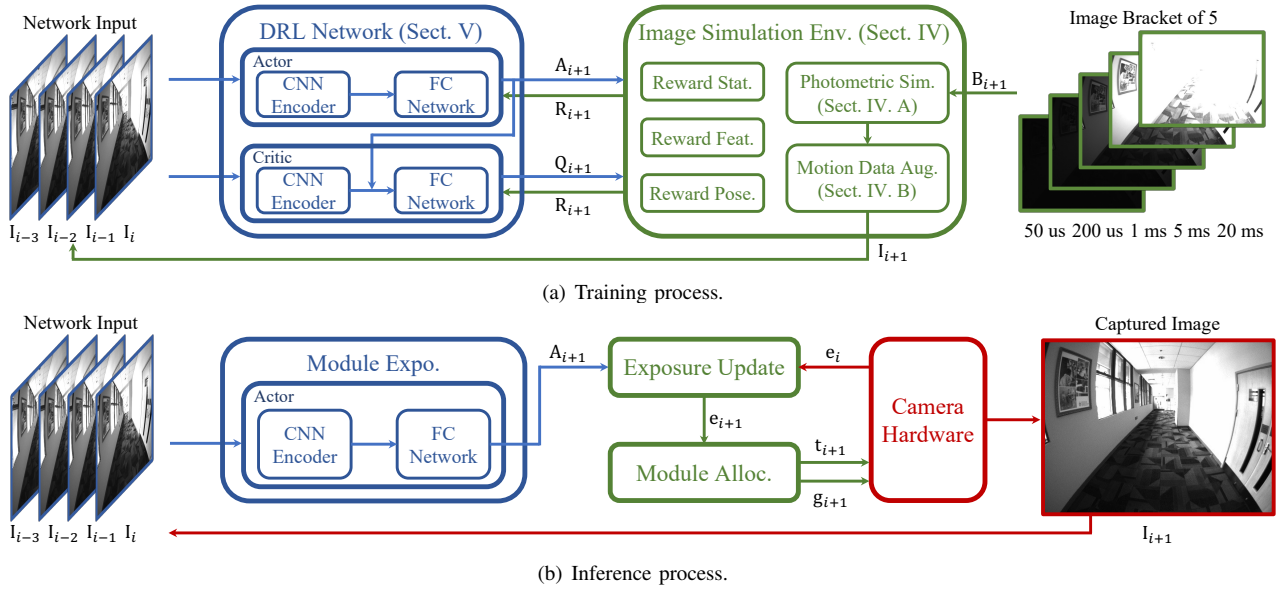


Fig. 2. System overview of the training and inference phases. In the training phase, we employ the image bracketing technique for simulation, enhanced by data augmentation to diversify sequence motion. The Soft Actor-Critic (SAC) framework was adopted for our DRL implementation. Within this framework, agents (actors) of varying intelligence levels were trained using distinct reward designs. In the inference phase, these trained agents generate a continuous relative action signal, which is then translated into target exposure for the next image. These control signals, comprising both exposure time and analog gain, are allocated via a rule-based strategy before transmission to the camera hardware. The newly captured image is subsequently fed back into the agent’s input for ongoing inference.

### III. SYSTEM OVERVIEW

#### A. Traditional Problem Formulation

Camera exposure control can be conceptualized as an optimization problem, formally expressed as

$$e_{i+1} = \arg \max_e \mathbf{M}(\mathbf{I}(e_i)), \quad (1)$$

where  $e$  denotes the *exposure*, a composite variable defined by exposure time  $t$  and analog gain  $g$

$$e = t \times 10^{\frac{g}{20}}. \quad (2)$$

Upon determining the optimal exposure  $e$ , an attribute allocation decomposes the exposure back into its constituent parameters, exposure time and analog gain, which are then used to adjust the camera’s hardware settings directly. The function  $\mathbf{I}(\cdot)$  denotes the imaging process that yields an image  $\mathbf{I}_i$  for a specified exposure, while  $\mathbf{M}(\cdot)$  assesses an image according to pre-defined metrics, such as gradient magnitude [3], [4], entropy [5], [6] and their combinations.

To address this optimization, feedback control methods compute an update increment  $\Delta e$  using the derivative  $\frac{\partial \mathbf{M}}{\partial e} = \frac{\partial \mathbf{M}}{\partial \mathbf{I}} \cdot \frac{\partial \mathbf{I}}{\partial e}$ . These methods necessitate a fully differentiable chain, and require multiple updates to converge to the optimal solution. Alternatively, function-fitting methods derive the reverse function of imaging process,  $\mathbf{I}^{-1}(\cdot)$ . By employing image synthesis techniques, these methods sample several seed exposures to generate corresponding images, thereby revealing the function  $\mathbf{M}(\cdot)$  through these samples. Although more time-consuming, these methods can determine the optimal exposure in a single update.

#### B. Our System Design

In this work, we employ DRL to train agents for camera exposure control. Existing research [1], [2] directly outputs the dual control parameters from the agent network, requiring a fully online interactive scheme, which is both time-consuming and inefficient. We split the exposure control problem into two distinct modules. The first module, referred as **ModuleExpo**, determines the optimal exposure  $e$  for the coming image, formulated as

$$e_{i+1} = \mathbf{ModuleExpo}(\mathbf{I}_{i-n+1:i}). \quad (3)$$

**ModuleExpo** processes a sequence of  $n$  historical images as input. This module is offline trained by a DRL framework with our environment simulator. The second module **ModuleAlloc** performs the attribute allocation role as

$$t_{i+1}, g_{i+1} = \mathbf{ModuleAlloc}(\mathbf{I}_{i-n+1:i}, e_{i+1}). \quad (4)$$

While not the primary focus of this work, this module is implemented using either the progressive strategy from our previous work [7] or a motion-awareness method [5].

Our framework design enables the training completely offline, avoiding online interaction with real-world scenarios. This approach significantly enhances the efficiency of data collection and training, rendering it more feasible for practical applications. It enhances the efficiency of data collection and training and makes it more feasible in practical applications. In subsequent sections of this paper, we will introduce our simulator implementation in Sect. IV, detail the DRL design in Sect. V, and demonstrate the effectiveness of our methods through experiments in Sect. VI.

#### IV. IMAGING SIMULATION ENVIRONMENT

During the training phase, a simulated environment can efficiently mitigate the inefficiencies associated with direct agent interaction in real-world scenarios. While existing simulators like CARLA [14] and Isaac Gym [15] are capable of supporting our tasks, yet they prove cumbersome or exhibit a notable discrepancy between the simulated imagery and actual real-world conditions.

To better align with our specific requirements, we have developed a lightweight simulator, which facilitates the replay of captured image sequences under varied exposure settings. Additionally, we have incorporated a motion data augmentation module designed to increase the diversity of trajectories, utilizing a limited dataset of image sequences.

##### A. Photometric Synthesis Process

In the principles of imaging, exposure time  $t$  is determined by camera shutter, whereas analog gain  $g$  amplifies the electrical signal emanating from the sensor array. The process of image synthesis can be viewed as another *virtual amplification*; however, it cannot be directly applied to images due to the nonlinear transformation of electrical signals (or irradiance) into image intensities. Photometric calibration [16] is essential to elucidate the relationship between electrical signal and image intensity, termed as the camera response function (CRF). Typically, this relationship is characterized by an inverse mapping from image intensity to logarithmic irradiance, expressed as

$$\mathbf{G}(\mathbf{I}) = \ln e + \ln \mathbf{E}, \quad (5)$$

where  $\mathbf{E}$  denotes the irradiance associated with image  $\mathbf{I}$ , solely determined by the scene. Once the function  $\mathbf{G}(\cdot)$  and its inverse  $\mathbf{G}^{-1}(\cdot)$  are established, the synthesis process is

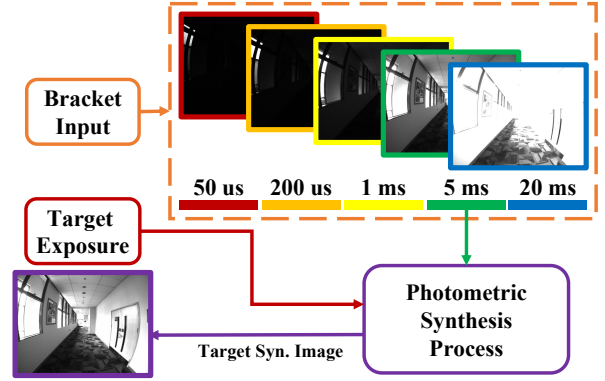
$$\mathbf{I}_1 = \max(0, \min(255, \mathbf{G}^{-1}(\mathbf{G}(\mathbf{I}_0) - \ln e_0 + \ln e_1))). \quad (6)$$

Further details can be found in our prior work [7].

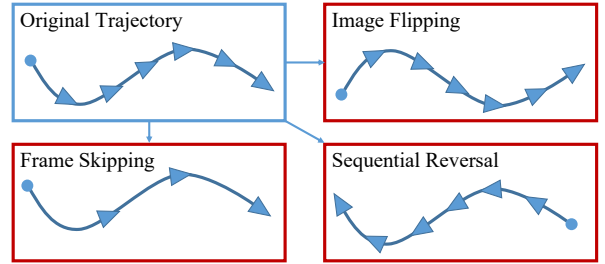
Inspired from Gamache *et al.* [17], we leverage bracketing image techniques to encompass a wide range of irradiances present within a scene. Specifically, we employ a bracketing capture consisting of 5 images (Fig. 3(a)) with exposure times of 50  $\mu$ s, 200  $\mu$ s, 1 ms, 5 ms, and 20 ms. Our previous research [7] indicates that the synthesis process encounters constraints when transitioning from long to short exposures, as data in over-exposed regions becomes irretrievable. Consequently, when an agent requires an image with a specific target exposure, we select the seed image whose exposure time is just below the target, and then serves it as the basis for synthesizing, thus enabling effective interaction.

##### B. Motion Augmentation

We realize the necessity of incorporating a broad spectrum of motion dynamics within our training datasets. However, once the training trajectories are collected, they remain invariant. Additionally, employing a bracketing technique to widen the range of irradiance inherently diminishes the simulator’s frame rate output. Specifically, using a bracket of 5 reduces the frame rate to one-fifth of the original



(a) Photometric synthesis process.



(b) Motion data augmentation.

Fig. 3. Our image simulation environment for DRL training. The photometric synthesis module enables offline interaction between the agents and captured image sequences. The motion data augmentation significantly enhances the diversity of available trajectories.

sequence rate. This reduction in frame rates indirectly affects the perceived speed of camera movement, thus introducing discrepancies between training and inference conditions.

To address the limited variability in trajectories, we implement several motion augmentation strategies (Fig. 3(b)). These strategies are randomly combined and introduced during training. **Image Flipping:** Horizontal and vertical flips are applied to entire sequences to simulate diverse motion patterns and orientations. **Speed Adjustment via Frame Skipping:** Frame skipping is employed to artificially increase the playback speed by factors of  $\times 1$ ,  $\times 2$ ,  $\times 3$ , enabling the simulation of various motion velocities. **Sequence Reversal:** Sequences are reversed to model entirely different behaviors. For instance, a sequence transitioning from dark to light can be inverted into a shift from light to dark.

Diverging from [2], we abstain from cropping images during data augmentation. By maintaining the integrity of the entire image frame, we facilitate the learning of lens distortion effects, enabling direct integration of these characteristics into the neural network.

#### V. REINFORCEMENT LEARNING FRAMEWORK DESIGN

The module **ModuleExpo** takes a segment of an image sequence as input and predicts the optimal exposure  $e$  for subsequent scenes. We evaluated both Soft Actor-Critic (SAC) and Proximal Policy Optimization (PPO) for policy training. While both algorithms completed the training process successfully, PPO demonstrated a faster training speed

but tended to converge to suboptimal policies. Consequently, we selected SAC as the preferred algorithm.

### A. State

Our system processes  $n = 4$  historical images as inputs, which are resized to  $84 \times 84$  pixels, yielding an input dimension of  $4 \times 84 \times 84$ . These inputs are first encoded by a CNN backbone consisting of three convolutional layers, integrated into the Actor and the Critic respectively. Both Actor and the Critic employ two fully connected layers as the head, featuring a hidden layer with a dimension of 512.

### B. Action

Continuous action spaces have been employed by both previous work [1], [2] due to their reduced need for update times compared to discrete spaces. Tomasi *et al.* implemented an absolute action update scheme, in which the agent determines the absolute exposure time  $t$  and gain  $g$ . We identify inefficiencies in this approach, as it needs referencing the exposure parameters of each image into the input to inform the network’s output. Additionally, the requirement for the action output to span all potential exposures complicates convergence with limited training samples. Lee *et al.* opted for a relative action update scheme, where the agent outputs a relative difference in action values.

We have developed a continuous-relative action scheme based on the concept of exposure compensation, quantified by the exposure value (EV) as

$$\text{EV} = \log_2 \frac{f^2}{t}, \quad (7)$$

where  $f$  represents the aperture value, and  $t$  is the exposure time. An EV increment of  $-1$  doubles the exposure time, whereas  $+1$  halves it. We define the action value range for EV between  $[-2, +2]$ , allowing each update to potentially increase or decrease the current exposure by up to fourfold.

### C. Reward

The design of the reward function is a pivotal component in reinforcement learning, as it directly influences the learning strategy of the agent. In this study, we investigated three distinct reward functions, each tailored to enhance convergence rates during training and to cultivate varying levels of agent intelligence.

1) *Statistical Reward*: The image statistical reward ( $\mathcal{R}_{stat}$ ) aims to optimize image brightness and stability, defined as

$$\mathcal{R}_{stat} = \mathcal{R}_{mean} - w_{f1k} \cdot \mathcal{R}_{f1k}, \quad (8)$$

where  $\mathcal{R}_{mean}$  quantifies the average image intensity, and  $\mathcal{R}_{f1k}$  addresses flickering, as discussed by [2]. The coefficient  $w_{f1k} = 0.2$  balances the smoothness of exposure control.

2) *Feature Reward*: The feature reward ( $\mathcal{R}_{feat}$ ) evaluates the effectiveness of feature point detection and tracking

$$\mathcal{R}_{feat} = w_{detect} \cdot \mathcal{R}_{detect} + w_{match} \cdot \mathcal{R}_{match}, \quad (9)$$

where  $\mathcal{R}_{detect}$  counts the detected feature points in the current frame, and  $\mathcal{R}_{match}$  is the number of features matched between

TABLE I  
HYPERPARAMETERS OF SAC TRAINING PHASE

Parameter	Value	Parameter	Value
Optimizer	Adam	Policy Distribution	Gaussian
Learning Rate	1e-4	Buffer Size	50000
Alpha Learning Rate	1e-4	Warm-up Size	5000
Batch Size	256	Discount Factor ( $\gamma$ )	0.99
Episode Length	500	Smooth Coefficient ( $\tau$ )	0.005

consecutive frames. The scaling coefficients  $w_{detect} = 0.005$  and  $w_{match} = 0.005$  ensure appropriate reward magnitudes, related to the feature numbers. Feature detection employs the ORB descriptor [18], and homography estimation refined with RANSAC filters outliers in feature matching.

3) *Pose Error Reward*: The pose error reward ( $\mathcal{R}_{pose}$ ) assesses the relative pose difference of VO systems by comparing it against ground truth data. The pose derived from images is denoted as  $\{\mathbf{R}_{img} \in \mathbb{S}\mathbb{O}(3), \mathbf{t}_{img} \in \mathbb{R}^3\}$ , encompassing both rotation and translation components. This pose is calculated using the two-frame reconstruction from ORB-SLAM [19], which involves computing the fundamental and homography matrices from matched points and deriving transformations from both. The pose with the minimal re-projection error is selected. A LiDAR-IMU odometry (LIO) system [20] outputs the ground truth trajectory, represented as  $\{\mathbf{R}_{gt} \in \mathbb{S}\mathbb{O}(3), \mathbf{t}_{gt} \in \mathbb{R}^3\}$ . The reward formulation is

$$\mathcal{R}_{pose} = -w_{rot} \cdot \mathcal{R}_{rot} - w_{trans} \cdot \mathcal{R}_{trans}, \quad (10)$$

where  $w_{rot} = 10$  and  $w_{trans} = 1$  serve as scaling factors. The translation error is defined by

$$\mathcal{R}_{trans} = \left\| \frac{\mathbf{t}_{img}}{\|\mathbf{t}_{img}\|_2} - \frac{\mathbf{t}_{gt}}{\|\mathbf{t}_{gt}\|_2} \right\|_2, \quad (11)$$

normalizing both translations before computing their Euclidean distance to account for scale discrepancies. The rotational error,  $\mathcal{R}_{rot}$ , is quantified in Lie algebra space [21]

$$\mathcal{R}_{rot} = \left\| (\log(\mathbf{R}_{img}^{-1} \cdot \mathbf{R}_{gt}))^\vee \right\|_2, \quad (12)$$

where  $\log(\cdot)$  denotes the matrix logarithm operator, and  $(\cdot)^\vee$  converts from Lie algebra to its vector space.  $\mathcal{R}_{rot}$  also means the rotation angle in radians. To cap the reward, its maximum value is set to 1, implying that rotation errors exceeding 57.3 degrees do not further penalize the agent.

## VI. EXPERIMENT

### A. Implementation Details

Our experimental setup depicted in Fig. 4, comprises a portable PC equipped with an Intel i3-n305 CPU of low power consumption. We selected two FLIR BFS 31S4C cameras, each fitted with a fisheye lens, to facilitate a wide field of view. To enhance image brightness in low-light conditions, we implemented a  $4 \times 4$  binning pattern, yielding an output resolution of  $512 \times 384$  pixels. One camera utilizes bracketing patterns to capture data for training and evaluation, while the other employs a built-in exposure method to serve as a reference during evaluation. A Livox

TABLE II

PERFORMANCE COMPARISON WITH ORB-SLAM3 USING RPE (MAX / RMSE). THE NUMBER OF RELOCALIZATION IS GIVEN IN BRACKET IF ANY. THE MARKER '-' REPRESENTS THE FAILURE CASES, CAUSED BY SYSTEM CRASH OR RMSE RPE GREATER THAN 1.0.

Sequence	Built-in	Shim	Zhang	DRL-stat	DRL-feat	DRL-pose	Dura. (s)	Vel. (m / s)	
Courtyard	×1	<b>1.42 / 0.29</b>	2.02 / 0.31	2.55 / 0.31	2.17 / 0.31	1.77 / 0.33	128.80	1.40	
	×2	- (1)	7.98 / 0.88	<b>1.64 / 0.49</b>	1.50 / 0.49	1.75 / 0.52	64.40	2.80	
Corridor	×1	1.98 / 0.22	2.24 / 0.24	2.19 / 0.24	1.96 / 0.23	<b>0.82 / 0.21</b>	173.50	0.93	
	×2	4.28 / 0.39 (1)	5.26 / 0.44 (1)	4.88 / 0.45 (1)	4.13 / 0.43 (1)	<b>1.29 / 0.32</b>	86.75	1.85	
Parking	×1	2.40 / 0.43	3.14 / 0.43	<b>1.44 / 0.42</b>	2.34 / 0.42	1.98 / <b>0.41</b>	128.00	1.71	
	×2	- (1)	- (1)	- (2)	- (3)	<b>1.84 / 0.62</b>	64.00	3.41	
Switch	×1	2.52 / 0.34 (1)	3.38 / 0.35 (1)	1.81 / 0.27 (1)	2.30 / 0.32 (1)	2.67 / 0.34 (1)	<b>1.65 / 0.23</b>	40.79	1.11



Fig. 4. Our experimental platform and training data scenarios in campus.

Mid-360 LiDAR integrated with a built-in IMU preforms a LIO system [20], served as the ground truth trajectory for VO system evaluation. Calibration of the intrinsic parameters of the cameras and the extrinsic parameters between the cameras and the IMU are conducted by using Kalibr [22].

The training datasets are captured on campus, as shown in Fig. 4. It comprises 3 sequences, including indoor and outdoor campus environments, as well as the underground parking lot, totaling 29 minutes and comprising 61653 images. The agents were trained using PyTorch on a PC with an Intel i9-13900k CPU and an Nvidia GeForce RTX 3080Ti GPU. The training process continued for 10000 episodes with network updates occurring every 50 frames. The hyperparameters for SAC is shown in Table I.

### B. Experiment: Visual Odometry

We evaluate the effectiveness and stability of different exposure control methods by processing image sequences through ORB-SLAM3 [19]. We generate exposure sequences using our simulator to ensure consistency in trajectories and image scenes, thereby mitigating errors due to variations in camera intrinsic and extrinsic parameters. Given the limitations of LIO in providing accurate global positioning, we adopt the relative pose error (RPE) as our evaluation metric, utilizing the *evo* toolbox [23]. We also record the number of failures and relocalizations across methods due to the challenging nature of the scenes. For our evaluation, we captured four distinct sequences, each representing different

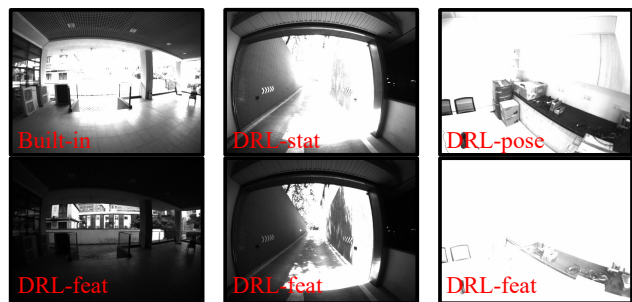


Fig. 5. Illustrations of different scenarios in our evaluation datasets.

lighting and environmental conditions:

- *Courtyard*: A typical VO environment with moderate lighting variations caused by the occlusions from surrounding buildings.
- *Corridor* and *Parking*: Both sequences feature significant lighting variations that challenge the exposure control methods, often leading to VO system failures.
- *Switch*: This sequence tests the responsiveness of the system to unpredictable, rapid light changes.

To prevent training overfitting, these evaluation sequences were collected in locations different from those used for training. For the sequences *Courtyard*, *Corridor*, and *Parking*, we increased the challenge by doubling the playback speed, as described in Sect. IV.

Several methods are implemented as the baseline comparison. **Built-in** is a feedback control method from FLIR cameras, aimed at optimizing average image brightness to a moderate value. **Shim** and **Zhang** are two methods target on optimizing image gradient magnitude, but with feedback control and function fitting schemes, respectively. Since we designed the three reward functions, we trained **DRL-stat**, **DRL-feat**, and **DRL-pose** for comparison.

Quantitative results are shown in Table II. In the *Courtyard* sequence, all methods perform well except for **Built-in** at double speed, which failed to adjust quickly enough to rapid motion (Fig. 5(a)), leading to over-exposure and tracking failures. In the sequences of *Corridor* and *Parking* with drastic lighting variations, **DRL-feat** shows the best performance, maintaining interframe tracking even under double

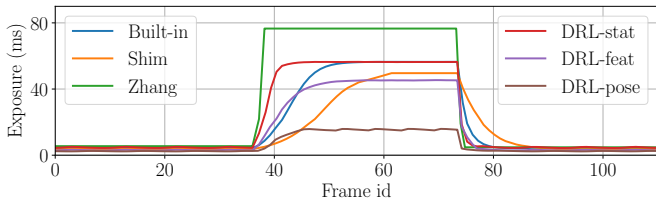


Fig. 6. The experiment of the reaction speed with a switch case of light off then on. The method of **Zhang** performs the fastest because of its principle of one step control. All our DRL methods (**DRL-stat**, **DRL-feat**, and **DRL-pose**) respond faster than feedback control methods (**Built-in** and **Shim**).

speed (Fig. 5(b)). In the *Switch* sequence, characterized by unpredictable lighting changes of 4 times, all methods were interrupted by the most dramatic transition from dark to light, expect **DRL-pose**, shown in Fig.5(c). This is because **DRL-pose** prefers a lower exposure: **DRL-pose** aims to directly minimize inter-frame pose errors. This enhances the agent’s preference for stable structural features over unstable textural features, which are plentiful but less reliable. Low exposure settings help obscure textural features and prevent blooming effects around structural features, which are typically delineated by contrasts between light and dark areas.

Additionally, we conducted a static experiment in the *Switch* scene to compare the response speeds of different methods to abrupt unpredictable lighting changes. The response performance is illustrated in Fig. 6. The function fitting method from **Zhang** exhibited the quickest response. Our DRL-based methods, equivalent to the mechanism of feedback control, all respond faster than the traditional feedback control methods.

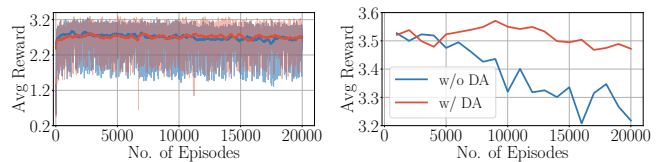
### C. Experiment: Data Augmentation

To assess the efficacy of our data augmentation module, we executed a controlled experiment wherein the **DRL-feat** agent was trained twice under identical hyperparameter settings. The only difference was the incorporation or exclusion of our motion augmentation module. Each agent underwent training across 20000 episodes, with the average reward per episode meticulously recorded. For evaluation purposes, model parameters were archived at every 1000 episode interval, and the average rewards were computed using the *Corridor* sequence. The results of this experiment are illustrated in Fig. 7.

After 2000 training episodes, a plateau in average rewards was observed for both agents. However, convergence was not attained as indicated by the *flickering* effect noted upon visual inspection of the *Corridor* sequences from both agents. As training advanced, the agent equipped with the data augmentation module demonstrated a reduction in flickering and maintained consistent reward levels. Conversely, the agent devoid of the data augmentation experienced intensified flickering and a gradual decrease in average rewards, indicating overfitting to the training data.

### D. Experiment: Time Consumption

Our training process does not necessitate any interaction with camera hardware or the real environment, rendering it



(a) Training process.

(b) Evaluation process.

Fig. 7. The trend of average reward alongside the number of training episodes. The agent training results with and without our motion data augmentation. To clearly see the training trend, we introduced a median filter with a size of 100. It can be seen that the training process without data augmentation (blue) has overfitting phenomenon, and the average reward on the evaluation keeps decreasing.

significantly faster than previous approaches [1], [2]. The training durations for our three agents—**DRL-stat**, **DRL-feat**, and **DRL-pose**—were 3 hours 13 minutes, 9 hours 35 minutes, and 10 hours 33 minutes, respectively, all trained for 10000 episodes. The average processing time per frame was recorded at 2.3 ms, 6.9 ms, and 7.6 ms, respectively.

We further evaluated the inference cost of our DRL framework against several baseline methods. All baseline implementations utilized C++ with O2 optimization. In contrast, our DRL models were executed simply by using PyTorch on the CPU of a handheld device. The results of this comparison are documented in Table III. The **Built-in** method exhibited the fastest performance due to its simpler computational operations. Our DRL agents significantly outpaced traditional methods and have the potential for further acceleration through software optimizations such as ONNX or TensorRT, or by leveraging dedicated camera hardware.

## VII. DISCUSSION

### A. Reward Designs

In this study, we designed three levels of reward functions, desiring to obtain different levels of intelligence for VO systems. **DRL-stat** focuses on optimizing average brightness and performs comparably to traditional algorithms. However, the DRL framework offers faster and more precise control responses. Since it does not incorporate high-level feature information, it lacks the capability to understand the scene comprehensively and preemptively adapt to changes. **DRL-feat** is designed to learn feature information with an objective to track as many feature points as possible. This capability enables it to comprehend motion trends and make predictions based on future static lighting conditions. However, it still suffers from overexposure during sudden, unpredictable light changes, though it recovers swiftly thanks to the DRL framework. **DRL-pose** does not yield superior VO performance, primarily due to two factors. First, it relies on additional pose ground truth data from a LIO system, whose accuracy may not always be sufficient. Unlike the first two models, which solely depend on images, this introduces potential external errors. Second, it focuses on minimizing pose errors between *adjacent* frames. Since these pose differences are minimal, triangulation errors can be significant. Although VO systems typically employ a keyframe technique to address this issue,

TABLE III  
RUNNING TIME COMPARISON

Method	Built-in <sup>1</sup>	Shim	Zhang	DRL
Time Consumption (ms)	0.39	11.77	15.09	1.58

<sup>1</sup> Since **Built-in** is implemented by camera hardware, we reimplemented it for time cost measurement.

attempts to integrate keyframe logic into the reward design did not result in model convergence. Keyframes led to sparse rewards, preventing the agent from receiving timely feedback.

### B. Exposure Allocation

We also attempted to train a DRL agent for exposure allocation. This can constrain its time cost, since allocation methods using optical flow [5] is usually time-consuming. Consequently, the entire exposure control pipeline became differentiable, allowing for the joint optimization of agents after their initial separate training phases.

For training the exposure allocation module, we implemented an online training with another SAC, and also tried an offline training using a deep Q-Network (DQN) based on parameter combinations from bracketing patterns. Both attempts employed our feature-level rewards. However, the agents were unable to develop stable or reasonable policies and failed to recognize blurring caused by camera motion.

The primary issue lies in the reward design, where a feature-level reward does not directly enhance the agent's perception of motion. We also explored image quality metrics related to motion blur. Given that each image lacks a reference ground truth, we were restricted to using non-reference image quality metrics, such as [24]. However, the result shows that this kind of non-reference metrics is fragile for DRL training, ultimately leading to the unsuccessful training of the allocation agent.

## VIII. CONCLUSION

In this work, we introduced deep reinforcement learning framework to train an exposure control agent for highly intelligent policies. By designing a lightweight image simulator, we successfully offlined the training process, greatly reducing the training difficulty and time. At the same time, we designed three different reward functions for the visual odometry tasks. The feature-level reward function enabled the agent to predict static lighting distribution and camera motion, and finally obtained advanced intelligence. Experiments proved the efficiency of our method, and the performance improvement for subsequent VO systems.

## REFERENCES

[1] J. Tomasi, B. Wagstaff, S. L. Waslander, and J. Kelly, "Learned camera gain and exposure control for improved visual feature detection and matching," *IEEE Robotics and Automation Letters*, vol. 6, no. 2, pp. 2028–2035, 2021.

[2] K. Lee, U. Shin, and B.-U. Lee, "Learning to control camera exposure via reinforcement learning," in *Proceedings of the IEEE/CVF Conference on Computer Vision and Pattern Recognition*, 2024, pp. 2975–2983.

[3] I. Shim, J.-Y. Lee, and I. S. Kweon, "Auto-adjusting camera exposure for outdoor robotics using gradient information," in *2014 IEEE/RSJ International Conference on Intelligent Robots and Systems*. IEEE, 2014, pp. 1011–1017.

[4] Z. Zhang, C. Forster, and D. Scaramuzza, "Active exposure control for robust visual odometry in hdr environments," in *2017 IEEE international conference on robotics and automation (ICRA)*. IEEE, 2017, pp. 3894–3901.

[5] B. Han, Y. Lin, Y. Dong, H. Wang, T. Zhang, and C. Liang, "Camera attributes control for visual odometry with motion blur awareness," *IEEE/ASME Transactions on Mechatronics*, 2023.

[6] J. Kim, Y. Cho, and A. Kim, "Proactive camera attribute control using bayesian optimization for illumination-resilient visual navigation," *IEEE Transactions on Robotics*, vol. 36, no. 4, pp. 1256–1271, 2020.

[7] S. Zhang, J. He, B. Xue, J. Wu, P. Yin, J. Jiao, and M. Liu, "An image acquisition scheme for visual odometry based on image bracketing and online attribute control," in *2024 IEEE International conference on robotics and automation (ICRA)*. IEEE, 2024.

[8] A. Romero, Y. Song, and D. Scaramuzza, "Actor-critic model predictive control," *arXiv preprint arXiv:2306.09852*, 2023.

[9] P. Cai, H. Wang, Y. Sun, and M. Liu, "Dq-gat: Towards safe and efficient autonomous driving with deep q-learning and graph attention networks," *IEEE Transactions on Intelligent Transportation Systems*, pp. 1–1, 2022.

[10] H. Jeong, H. Hassani, M. Morari, D. D. Lee, and G. J. Pappas, "Deep reinforcement learning for active target tracking," in *2021 IEEE International Conference on Robotics and Automation (ICRA)*. IEEE, 2021, pp. 1825–1831.

[11] N. Messikommer, G. Cioffi, M. Gehrig, and D. Scaramuzza, "Reinforcement learning meets visual odometry," *arXiv preprint arXiv:2407.15626*, 2024.

[12] J. Cheng, Y. Chen, and Q. Chen, "Pluto: Pushing the limit of imitation learning-based planning for autonomous driving," *arXiv preprint arXiv:2404.14327*, 2024.

[13] J. Xing, A. Romero, L. Bauersfeld, and D. Scaramuzza, "Bootstrapping reinforcement learning with imitation for vision-based agile flight," *arXiv preprint arXiv:2403.12203*, 2024.

[14] A. Dosovitskiy, G. Ros, F. Codevilla, A. Lopez, and V. Koltun, "Carla: An open urban driving simulator," in *Conference on robot learning*. PMLR, 2017, pp. 1–16.

[15] J. Liang, V. Makoviychuk, A. Handa, N. Chentanez, M. Macklin, and D. Fox, "Gpu-accelerated robotic simulation for distributed reinforcement learning," in *Conference on Robot Learning*. PMLR, 2018, pp. 270–282.

[16] P. E. Debevec and J. Malik, "Recovering high dynamic range radiance maps from photographs," in *ACM SIGGRAPH 2008 classes*, 2008, pp. 1–10.

[17] O. Gamache, J.-M. Fortin, M. Boxan, F. Pomerleau, and P. Giguère, "Exposing the unseen: Exposure time emulation for offline benchmarking of vision algorithms," *arXiv preprint arXiv:2309.13139*, 2023.

[18] E. Rublee, V. Rabaud, K. Konolige, and G. Bradski, "Orb: An efficient alternative to sift or surf," in *2011 International conference on computer vision*. IEEE, 2011, pp. 2564–2571.

[19] C. Campos, R. Elvira, J. J. G. Rodríguez, J. M. Montiel, and J. D. Tardós, "Orb-slam3: An accurate open-source library for visual, visual-inertial, and multimap slam," *IEEE Transactions on Robotics*, vol. 37, no. 6, pp. 1874–1890, 2021.

[20] K. Chen, B. T. Lopez, A.-a. Agha-mohammadi, and A. Mehta, "Direct lidar odometry: Fast localization with dense point clouds," *IEEE Robotics and Automation Letters*, vol. 7, no. 2, pp. 2000–2007, 2022.

[21] J. Sola, J. Deray, and D. Atchuthan, "A micro lie theory for state estimation in robotics," *arXiv preprint arXiv:1812.01537*, 2018.

[22] J. Rehder, J. Nikolic, T. Schneider, T. Hinzmann, and R. Siegwart, "Extending kalibr: Calibrating the extrinsics of multiple imus and of individual axes," in *2016 IEEE International Conference on Robotics and Automation (ICRA)*. IEEE, 2016, pp. 4304–4311.

[23] H. Rebecq, T. Horstschäfer, G. Gallego, and D. Scaramuzza, "Evo: A geometric approach to event-based 6-dof parallel tracking and mapping in real time," *IEEE Robotics and Automation Letters*, vol. 2, no. 2, pp. 593–600, 2016.

[24] F. Crete, T. Dolmiere, P. Ladret, and M. Nicolas, "The blur effect: perception and estimation with a new no-reference perceptual blur metric," in *Human vision and electronic imaging XII*, vol. 6492. SPIE, 2007, pp. 196–206.